






Capturing near-field circular dichroism enhancements from far-field measurements

Jorge Olmos-Trigo ^{1,*} Jon Lasa-Alonso ^{2,3,4} Iker Gómez-Viloria ³
Gabriel Molina-Terriza ^{2,3,5} and Aitzol García-Etxarri ^{2,5}

¹*Departamento de Física, Universidad de La Laguna, Apdo. 456, E-38200 San Cristóbal de La Laguna, Spain*

²*Donostia International Physics Center, Paseo Manuel de Lardizabal 4, 20018 Donostia-San Sebastian, Spain*

³*Centro de Física de Materiales, Paseo Manuel de Lardizabal 5, 20018 Donostia-San Sebastian, Spain*

⁴*Departamento de Ciencias Básicas, Mondragon Unibertsitatea, Loramendi 4, 20500 Arrasate, Spain*

⁵*IKERBASQUE, Basque Foundation for Science, María Díaz de Haro 3, 48013 Bilbao, Spain*



(Received 24 October 2022; accepted 14 December 2023; published 8 February 2024)

Molecular circular dichroism (CD) spectroscopy faces significant limitations due to the inherent weakness of chiroptical light-matter interactions. In this view, resonant optical antennas constitute a promising solution to this problem, since they can be tuned to increase the CD enhancement factor, f_{CD} , a magnitude describing the electromagnetic near-field enhancement of scatterers associated with a given helicity. However, an exact analytical expression of f_{CD} remains elusive. Here, we derive an exact multipolar expansion of f_{CD} , which is valid to deduce the integrated near-field CD enhancements of chiral molecules in the presence of scatterers of any size and shape under general illumination conditions. Our exact analytical findings extend previous approximate expressions of f_{CD} that are restricted to the dipolar regime. In addition to this, and based on our exact analytical findings, we show that the near-field f_{CD} factor can be related to magnitudes that can be computed in the far field, i.e., the scattering cross-section and the helicity expectation value. Strikingly, we show that in the case of lossless cylindrically symmetric samples, the near-field f_{CD} factor can be inferred experimentally only from two far-field measurements at specific scattering angles. Our contribution paves the way for the experimental characterization of devices capable of enhancing molecular CD spectroscopy from far-field measurements.

DOI: [10.1103/PhysRevResearch.6.013151](https://doi.org/10.1103/PhysRevResearch.6.013151)

Chirality is a geometrical property of objects which are not superimposable with its mirror image. Chiral objects are ubiquitous in nature. Many organic molecules, such as glucose and most biological amino acids, are chiral. Not to mention the DNA double helix, which, in its standard form, always twists like a right-handed screw [1]. In the pharmaceutical industry, chiral specificity is critical because opposite enantiomers, i.e., mirror pairs of chiral molecules, can have beneficial or detrimental biological effects on our organism depending on their handedness. Even if they share the same atomic composition, enantiomer pairs are indistinguishable when measuring their scalar molecular properties. Their chiral nature is revealed only when interacting with other chiral entities.

In electromagnetism, the most common chiral observable is helicity [2]. Chiral molecules show a preferential absorption for fields of opposite helicities (left- or right-handed polarized waves with helicity eigenvalues of $\sigma = \pm 1$). In a conventional Circular dichroism (CD) spectroscopy setup, a chiral molecular solution is sequentially illuminated by fields of opposite helicities, and the total transmitted power is recorded for each case. The CD signal is then computed by taking

the difference between these two power measurements in transmission. However, the inherent weakness of chiroptical responses strongly limits the sensitivity of CD spectroscopy.

Optical antennas, designed to control the properties of light [3], are promising candidates to enhance the spectroscopic signals of chiral samples. The underlying phenomenon is that optical antennas can be engineered to enhance electromagnetic fields while preserving the electromagnetic helicity [4–6]. Many works have explored optical antennas [7–9] and metasurfaces, namely, flat planar arrays of optical antennas, made of metallic [10–13] or/and high refractive index materials [14,15] for enhanced chiral sensing, meaning, enhancing the CD signal of the measured chiral molecules [16–21]. Examples of such works can be found in the ultraviolet [22], visible [23–29], or near -and far-infrared spectral range [30–36].

Moreover, and quite recently, optical cavities have also been proposed as efficient platforms for enhanced chiral sensing [37–39]. However, researchers rely on numerical methods to design enhanced chiral sensing devices, as capturing the vector character of the near-field contribution can be challenging. In this work, we derive an exact multipolar expansion of f_{CD} , which is valid to deduce the integrated near-field CD enhancements of chiral molecules in the presence of scatterers of any size and shape under general illumination conditions. To the best of our knowledge, this is the most general expression of f_{CD} that can be found in the literature.

Based on analytical findings, we demonstrate that f_{CD} is proportional to the product of the scattering cross-section and

*jolmostrijo@gmail.com

Published by the American Physical Society under the terms of the [Creative Commons Attribution 4.0 International](https://creativecommons.org/licenses/by/4.0/) license. Further distribution of this work must maintain attribution to the author(s) and the published article's title, journal citation, and DOI.

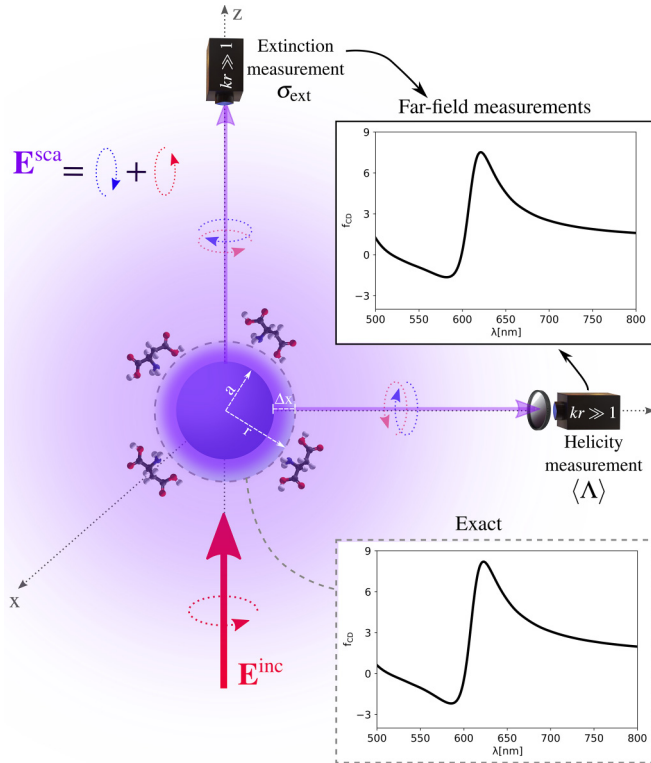


FIG. 1. Scattering process in which an incident field with well-defined helicity (red beam) impinges on an optical (achiral) antenna, represented by a Silicon sphere of radii $a = 75$ nm. The dashed region represents the integrating sphere $r = 76$ nm where the exact f_{CD} is calculated. Enantiomers are also depicted surrounding the integrating sphere. Two measurements are proposed to capture CD enhancements: Exact f_{CD} computed from Eq. (8) and f_{CD} computed from a far-field measurement [see Eq. (18)] of extinction σ_{ext} ($\theta = 0$) and helicity $\langle \Lambda \rangle$ at the right-angle ($\theta = 90$).

the helicity expectation value, both of which can be measured experimentally in the far-field limit. This enables us to bridge near-field magnitudes, such as f_{CD} , to experimentally accessible Stokes parameters in the far field for the first time. In addition to this, we reveal that it is possible to infer f_{CD} for lossless and cylindrically symmetric scatterers using only two far-field measurements: the extinction cross-section and the helicity density at specific scattering angles θ . This is particularly noteworthy for dipolar achiral antennas under plane-wave illumination, which is the most commonly studied scenario in the field of chiral light-matter interactions. In this particular case, we anticipate that the two required scattering angles to capture f_{CD} in far field are the forward $\theta = 0^\circ$ (for computing extinction) and the right angle $\theta = 90^\circ$ (for obtaining helicity). In this regard, please check Fig. 1 for further clarification.

Let us now introduce the theoretical framework of our work. To describe the excitation of chiral molecules, we adopt the formalism introduced by Tang and Cohen [40]. The CD signal of a chiral molecule under the illumination of a well-defined helicity field ($\sigma = \pm 1$) can be computed in vacuum as

$$CD_{inc}(\mathbf{r}) = -\frac{4}{\varepsilon} \text{Im}\{G\} C_{inc}^\sigma(\mathbf{r}), \quad (1)$$

where G is the chiral polarizability of the molecule and $C_{inc}^\sigma(\mathbf{r})$ is the incident local density of optical chirality [40],

$$C_{inc}^\sigma(\mathbf{r}) = \frac{k\varepsilon}{2} \text{Im}\{\mathbf{E}_{inc}^\sigma(\mathbf{r}) \cdot \mathbf{Z}\mathbf{H}_{inc}^{\sigma*}(\mathbf{r})\}. \quad (2)$$

Here, k is the radiation wave number, ε is the electric permittivity of the medium. Moreover, $\mathbf{E}_{inc}^\sigma(\mathbf{r})$ and $\mathbf{H}_{inc}^\sigma(\mathbf{r})$ refer to incident electromagnetic fields with well-defined helicity [41] (see Appendix A 1 for more details).

In the presence of optical antennas (see Fig. 1) and in the helicity basis [42], the total electromagnetic fields can be generally written as $\mathbf{E}_{tot}^{\sigma\sigma'}(\mathbf{r}) = \mathbf{E}_{sca}^{\sigma\sigma'}(\mathbf{r}) + \mathbf{E}_{inc}^\sigma(\mathbf{r})\delta_{\sigma\sigma'}$. Here $\mathbf{E}_{sca}^{\sigma\sigma'}(\mathbf{r})$ is the scattered electromagnetic field written in terms of the electromagnetic modes with well-defined helicity $\sigma' = \pm 1$ (see Appendix A 2 for more details). In analogy with Eq. (1), we can express the total CD signal of a chiral molecule in the presence of an optical antenna as [43]

$$CD_{tot}(\mathbf{r}) = -\frac{4}{\varepsilon} \text{Im}\{G\} C_{tot}^\sigma(\mathbf{r}) = \frac{k}{2} \text{Im}\{G\} \sum_{\sigma'=\pm 1} \sigma' |\mathbf{E}_{tot}^{\sigma\sigma'}(\mathbf{r})|^2. \quad (3)$$

We seek to maximize $CD_{tot}(\mathbf{r})$ with Eq. (3). However, such enhancements cannot be achieved through G since it is a fixed chiral molecular parameter that cannot be engineered upon illumination. In contrast, the total density of optical chirality, $C_{tot}^\sigma(\mathbf{r})$, can be tuned to enhance light-matter interactions and, thus, increase the sensitivity of CD spectroscopy [44]. To get a deeper insight into the total density of optical chirality, let us split $C_{tot}^\sigma(\mathbf{r})$ into three contributions; namely, $C_{tot}^\sigma(\mathbf{r}) = C_{inc}^\sigma(\mathbf{r}) + C_{sca}^\sigma(\mathbf{r}) + C_{int}^\sigma(\mathbf{r})$, with

$$C_{inc}^\sigma(\mathbf{r}) = \sigma |\mathbf{E}_{inc}^\sigma(\mathbf{r})|^2, \quad (4)$$

$$C_{sca}^\sigma(\mathbf{r}) = |\mathbf{E}_{sca}^{\sigma+}(\mathbf{r})|^2 - |\mathbf{E}_{sca}^{\sigma-}(\mathbf{r})|^2, \quad (5)$$

$$C_{int}^\sigma(\mathbf{r}) = 2\sigma \text{Re}\{\mathbf{E}_{inc}^{\sigma*}(\mathbf{r}) \cdot \mathbf{E}_{sca}^{\sigma\sigma}(\mathbf{r})\}. \quad (6)$$

Here $C_{sca}^\sigma(\mathbf{r})$ and $C_{int}^\sigma(\mathbf{r})$ account for the scattering and interference contributions to the optical chirality in the presence of achiral optical antennas, respectively. Now, it is experimentally challenging to place enantiomers at will, namely, at a desired spatial coordinate \mathbf{r} . Accordingly, it is more convenient to introduce an averaged expression of the local CD enhancement factor that gives insight into how efficient the optical antenna might be at enhancing CD spectroscopy [34]. To that end, let us first integrate both Eqs. (1) and (3) over an imaginary sphere of radius r surrounding the optical antenna to then calculate the ratio between these integrals, namely,

$$f_{CD} = \frac{\int CD_{tot}(\mathbf{r}) dS}{\int CD_{inc}(\mathbf{r}) dS} = 1 + \frac{\int C_{sca}^\sigma(\mathbf{r}) dS + \int C_{int}^\sigma(\mathbf{r}) dS}{\int C_{inc}^\sigma(\mathbf{r}) dS}, \quad (7)$$

where $dS = r^2 \sin\theta d\varphi d\theta$. To compute Eq. (7), we need the orthogonality relations that the incident and scattered electromagnetic fields satisfy when written in terms of the multipoles with well-defined helicity. Fortunately, these can be derived from Jackson's book in its third edition [45] (see Appendix B 1 for the explicit derivation).

Now, by considering these relations, and after some algebra (see Appendix B 2 for more details), we arrive at

$$f_{\text{CD}} = 1 + \frac{\tilde{C}_{\text{sca}}^\sigma + \tilde{C}_{\text{int}}^\sigma}{\tilde{C}_{\text{inc}}^\sigma}, \quad (8)$$

where

$$\tilde{C}_{\text{inc}}^\sigma = \sigma \sum_{lm} |C_{lm}^\sigma|^2 G_{j_l j_l}, \quad (9)$$

$$\tilde{C}_{\text{sca}}^\sigma = -2 \sum_{lm} \text{Im}\{C_{lm}^\sigma b_{lm}^{\sigma*}\} G_{h_l h_l}, \quad (10)$$

$$\tilde{C}_{\text{int}}^\sigma = \sqrt{2} \sum_{lm} \text{Re}\{C_{lm}^{\sigma*} (a_{lm}^\sigma - i\sigma b_{lm}^\sigma) G_{j_l h_l}\}. \quad (11)$$

Here \tilde{C} denotes the average of C over a spherical surface, a_{lm}^σ and b_{lm}^σ are the electric and magnetic scattering coefficients of an arbitrary sample while C_{lm}^σ denotes the incident coefficients characterizing the nature of the wave. Moreover,

$$G_{f_l g_l} = \frac{1}{2} \left(2f_l^*(u)g_l(u) + \frac{1}{u^2} \frac{\partial}{\partial u} \left\{ u f_l^*(u) \frac{\partial}{\partial u} [u g_l(u)] \right\} \right). \quad (12)$$

Here $G_{f_l g_l}$ is a scalar function that depends on spherical Bessel and Hankel functions. In particular, we may have $\{f_l, g_l\} = \{j_l, j_l\}, \{h_l, h_l\}, \{j_l, h_l\}$, j_l and h_l being the spherical Bessel and Hankel functions, respectively [45]. Note that $u = kr$ represents the normalized radius of an imaginary sphere surrounding the achiral object, where the averaging integral is carried out. For the mathematical details, please check Appendix B 1.

Equation (8), together with Eqs. (9)–(12), is one of the first main results of this paper. These equations describe the integrated CD enhancement in the presence of scatterers of any size and shape under the excitation of fields with well-defined helicity. Our results overcome previous approximations, such as the widely used system of a circularly polarized plane-wave illuminating dipolar objects [25–36]. In this regard, it is crucial to highlight that the results we have obtained, as summarized in Eqs. (8)–(12), represent an extension of prior analytical (but approximate) expressions for f_{CD} [8,27,46]. These previous expressions of the f_{CD} factor were originally derived within the dipolar regime, considering fields in the near-field limit with f_{CD} scaling as $1/(kr)^6$, and were established under the illumination of a circularly polarized plane wave. Thus, our findings, summarized in Eqs (8)–(12), may find applications in chiral sensing and chiral spectroscopy techniques beyond the current state-of-the-art.

To get a deeper insight into the generality of our results, let us briefly comment on some aspects of f_{CD} with respect to chiral molecules. In our study of dipolar chiral molecules, we must consider the multipolar contributions of the incoming field in the f_{CD} factor. This is true even though chiral molecules only react to the local values of the electric and magnetic fields, neglecting derivatives of the fields that would play a role with quadrupolar transitions in the chiral molecule. This is because chiral molecules are placed outside the sphere surrounding the origin of coordinates, where the optical antenna is located. In short, the description of the f_{CD} outside

the origin requires the full multipolar distribution of the field, especially if the point is at a distance large compared with the wavelength.

At this point, we provide the steps to find f_{CD} around any optical antenna:

(1) First, we need the solution of the electromagnetic fields under the illumination of a well-defined helicity beam. These can be obtained by any Maxwell's solver.

(2) Then, we project in the far field the exact solution of the scattered fields to obtain the scattering coefficients (see Eq. (9.123) in Jackson's book in its third edition [45]).

(3) Finally, we can compute f_{CD} via Eq. (8), together with Eqs. (9)–(12).

Let us briefly state the practical value of our work. On the theoretical side, we might notice that we can directly compute the f_{CD} factor from the exact solution of the fields under the illumination of a well-defined helicity beam using standard Maxwell solvers. However, we would lose track of the role of the multipoles contributing to the f_{CD} factor. Moreover, by using standard Maxwell solvers, imaginary integrating spheres surrounding the object would be needed at each calculation of the fields to perform the averaging integral surrounding the object. In contrast, our formalism allows inferring the role of the multipoles contributing to the f_{CD} factor, which is an averaged magnitude itself.

From an experimental perspective, one approach to optimize the design of an optical antenna so that it maximizes the CD spectra of chiral molecules would be to measure iteratively the CD signal of suspended chiral molecules with and without different antenna designs. However, this trial-and-error optimization procedure would require multiple measurements and, thus, would not be cost-effective. Our results, which are based on Eq. (8), along with Eqs. (9)–(12), offer a far more efficient method to optimize optical antenna designs for enhanced CD spectroscopy without the need to perform multiple CD experiments with suspended chiral molecules in the presence of the designed structures.

As an illustrative example of our method and based on the aforementioned recipe, we depict the exact expression of f_{CD} for a sphere sustaining several multipoles under plane-wave illumination [see Fig. 2(a)]. Note that in Fig. 2, we have defined $u = kr = k(a + \delta_x)$, being $\delta_x = 1$ nm the increment with respect to the radius a of the achiral sphere. As a result, we calculate f_{CD} in the near field. Moreover, we also depict in Fig. 2(b) the scattering contribution to f_{CD} . That is, $f_{\text{CD}} - \tilde{C}_{\text{int}}^\sigma / \tilde{C}_{\text{inc}}^\sigma$. From now on, the latter quantity will be referred to as the scattering approximation. For the sake of clarity, we summarize the exact multipolar expansion and the scattering approximation of f_{CD} for Mie scatterers under the illumination of a circularly polarized plane wave in Table I. Now, we infer, by comparing Fig. 2(a) with Fig. 2(b), that the exact solution of f_{CD} can be fairly approximated to just the scattering approximation. We understand the validity of the scattering approximation of f_{CD} based on the following:

(1) On mathematical grounds, and according to Eq. (B3), it can be checked that $G_{h_l h_l} \gg |G_{j_l h_l}|$ for $u < l$. That is, fundamental properties of spherical Bessel functions dictate that the scattering contribution dominates over the interference term for $u < l$.

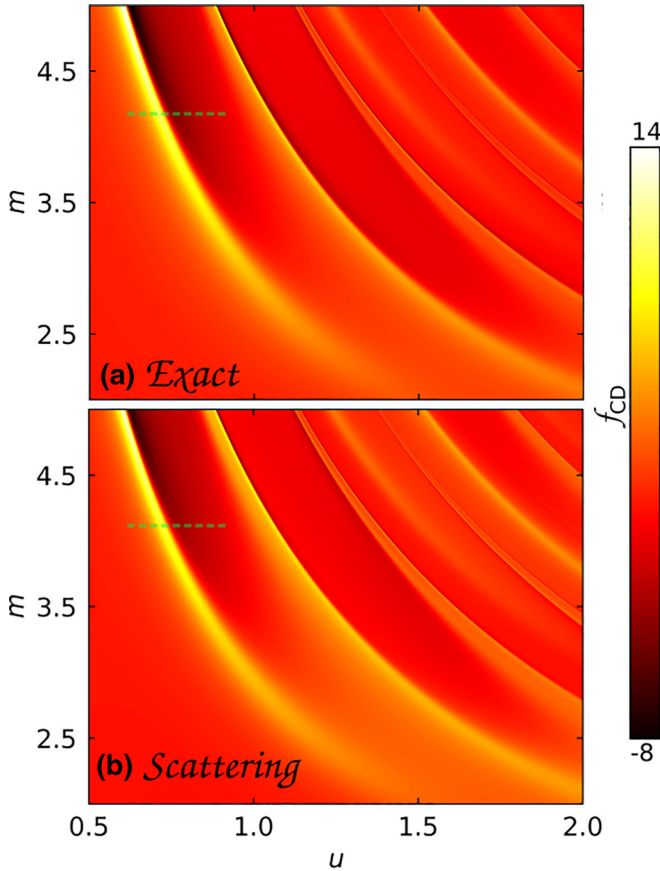


FIG. 2. CD enhancements for achiral sphere under the illumination of a circularly polarized plane-wave. (a) f_{CD} (exact) and (b) $f_{CD} - \tilde{C}_{\text{int}}^{\sigma} / \tilde{C}_{\text{inc}}^{\sigma}$ (scattering). Here $u = kr = k(a + \delta_x)$, with $\delta_x = 1$ nm, ka being the optical size and m the refractive index contrast. The exact and scattering multipolar expansions for Mie scatterers are given in Table I. The dashed green lines correspond to a cut depicted in Fig. 3.

(2) On physical grounds, we notice that there are no strong resonances of the l th multipole for $u > l$. For example, dipolar and quadrupolar resonances typically arise for $u < 1$ and $1 < u < 2$, respectively.

At this point, we will delve into Eq. (10), which approximates the efficiency of an optical antenna to enhance the f_{CD} factor. In particular, let us examine its physical meaning when

TABLE I. Analytic expressions for the CD enhancement factor, f_{CD} , depending on the interaction between an incident plane-wave and an achiral spherical particle. Here a_l and b_l denote the electric and magnetic scattering Mie coefficients [47] and $\{G_{h_l h_l}, G_{j_l h_l}\}$ can be computed from Eq. (12); Λ_{θ} the helicity density; σ_{sca} and σ_{ext} are the scattering and extinction cross-sections; and λ the radiation wavelength.

| Approximation in the calculation of f_{CD} | Plane wave illumination |
|--|---|
| Exact multipolar expansion [see Fig. 2(a)] | $f_{CD} = 1 + \sum_l (2l + 1) (\text{Re}\{a_l b_l^*\} G_{h_l h_l} - \text{Re}\{(a_l + b_l) G_{j_l h_l}\})$ |
| Scattering approximation [see Fig. 2(b)] | $f_{CD} \sim 1 + \sum_l (2l + 1) \text{Re}\{a_l b_l^*\} G_{h_l h_l}$ |
| Scattering approximation for arbitrary samples well-described by a single multipolar order l | $f_{CD} \sim 1 + \frac{\pi G_{h_l h_l}}{\lambda^2} \langle \Lambda \rangle \sigma_{\text{sca}} \xrightarrow{\text{Lossless}} f_{CD} \sim 1 + \frac{\pi G_{h_l h_l}}{\lambda^2} \langle \Lambda \rangle \sigma_{\text{ext}}$ |
| Scattering approximation for cylindrical samples well-described by a single multipolar order l and total angular momentum m (see Fig. 3) | $f_{CD} \sim 1 + \frac{\pi G_{h_l h_l}}{\lambda^2} \Lambda_{\theta} \sigma_{\text{sca}} \xrightarrow{\text{Lossless}} f_{CD} \sim 1 + \frac{\pi G_{h_l h_l}}{\lambda^2} \Lambda_{\theta} \sigma_{\text{ext}}$ |

just one multipole order (electric and magnetic) contributes to the optical response of the antenna. In this regard, it is essential to note that the one multipole approximation includes the most studied scenario by the nanophotonic community devoted to enhanced chiral sensing: a circularly polarized plane wave incident on dipolar objects [25–36].

Now, when the optical response of the antenna can be described by just one multipole order l , Eq. (10) reads

$$\tilde{C}_{\text{sca}}^{\sigma} = -2G_{h_l h_l} \sum_{m=-l}^{m=l} \text{Im}\{a_{lm}^{\sigma} b_{lm}^{\sigma*}\}. \quad (13)$$

By inspecting Eq. (13), we notice that $\tilde{C}_{\text{sca}}^{\sigma}$ is proportional to $G_{h_l h_l}$ (evaluated in the near field), and the interference between the electric and magnetic scattering coefficients $\text{Re}\{a_{lm}^{\sigma} b_{lm}^{\sigma*}\}$. Now, let us introduce the (V/I)-Stokes parameter, which can be inferred using conventional waveplates in the far field [48,49]. That is, let us introduce the normalized (and unit-less) electromagnetic helicity expectation value, which reads [50–52]

$$\langle \Lambda \rangle = \frac{\int_{\Omega} (|\mathbf{E}_{\text{sca}}^{\sigma+}|^2 - |\mathbf{E}_{\text{sca}}^{\sigma-}|^2) d\Omega}{\int_{\Omega} (|\mathbf{E}_{\text{sca}}^{\sigma+}|^2 + |\mathbf{E}_{\text{sca}}^{\sigma-}|^2) d\Omega}. \quad (14)$$

Computing $\langle \Lambda \rangle$ in the case in which the optical response can be described by a single multipolar order l [50–52], we can write

$$\langle \Lambda \rangle = -2 \frac{\sum_m \text{Im}\{a_{lm}^{\sigma} b_{lm}^{\sigma*}\}}{\sum_m (|a_{lm}^{\sigma}|^2 + |b_{lm}^{\sigma}|^2)} = -2 \frac{\sum_m \text{Im}\{a_{lm}^{\sigma} b_{lm}^{\sigma*}\}}{k^2 \sigma_{\text{sca}}}, \quad (15)$$

where σ_{sca} is the scattering cross section [47,53]. At this point, we notice that the expression for $\tilde{C}_{\text{sca}}^{\sigma}$ resembles $\langle \Lambda \rangle$. In fact, and without loss of generality, we can write $\tilde{C}_{\text{sca}}^{\sigma} = G_{h_l h_l} \langle \Lambda \rangle k^2 \sigma_{\text{sca}}$. As a result, f_{CD} yields

$$f_{CD} \sim 1 + \frac{\tilde{C}_{\text{sca}}^{\sigma}}{\tilde{C}_{\text{inc}}^{\sigma}} = 1 + \frac{G_{h_l h_l} \langle \Lambda \rangle k^2 \sigma_{\text{sca}}}{\tilde{C}_{\text{inc}}^{\sigma}}. \quad (16)$$

This is another significant result of the present work. We have linked the averaged optical chirality associated with scattered fields, $\tilde{C}_{\text{sca}}^{\sigma}$, which is usually computed in the near field (through $G_{h_l h_l}$), with quantities that can be evaluated or

measured in far field, i.e., the helicity expectation value, $\langle \Lambda \rangle$ and the scattering cross-section, σ_{sca} .

Our findings align with previous works devoted to identifying far-field observables for characterizing chiral optical near fields [12]. In Ref. [12] the far-field observable is the optical chirality flux. In our work, we connect the averaged local density of chirality to the helicity expectation value and the scattering cross-section, quantities that can be directly inferred from measurements of the Stokes parameters [49].

At this stage, let us remark on a fundamental feature that is embedded in Eq. (16). For both lossless and helicity-preserving objects, we can write $\tilde{C}_{\text{sca}}^\sigma \sim G_{h_l h_l} k^2 \sigma_{\text{ext}}$, with $\sigma_{\text{ext}} = \sigma_{\text{sca}}$, σ_{ext} being the extinction cross-section [47]. That is, the CD enhancement captured by the f_{CD} factor is related to a single measurement of the extinct power in the forward direction whenever $\langle \Lambda \rangle \sim 1$. The relation between f_{CD} and σ_{ext} for helicity-preserving achiral objects significantly reduces eventual experimental and numerical calculations devoted to enhanced chiral sensing. As a matter of fact, a lossless, helicity-preserving, and cylindrically symmetry building block has shown to be desirable to achieve high values of f_{CD} , as shown, for instance, in Refs. [29,32,34].

So far, we have shown an alternative way to infer local CD enhancements close to the achiral antenna by computing far-field magnitudes such as the helicity expectation value, the scattering cross-section, or the extinction cross-section. In particular, a scenario of major interest for the purpose of enhanced chiral detection occurs when the achiral antenna preserves the helicity of the incident illumination, i.e., whenever $\langle \Lambda \rangle \sim 1$. Such objects satisfy $|\mathbf{E}_{\text{sca}}^{\sigma\sigma'}(\mathbf{r})| \sim 0$ for $\sigma \neq \sigma'$, thus, the local sign of optical chirality is preserved.

Experimentally, identifying helicity-preserving scatterers requires measuring the polarization of all the scattered field components, something which is not feasible in practice. Thus, our question is: can we infer the helicity expectation value, $\langle \Lambda \rangle$, from a single measurement of its local density in the far field? We will discuss scenarios in which the helicity density at a given scattering angle can be identical to its expected value. In particular, we will focus on cylindrically symmetric scatterers which preserve the total angular momentum in the incident direction ($m = m'$) and whose optical response can be well-described by a single multipolar order ($l = l'$), e.g., nanodisks at normal incidence or spherical particles under the illumination of tightly focused Laguerre-Gaussian beams [54].

Mathematically, we can express the aforementioned condition as $\langle \Lambda \rangle = \Lambda_\theta$, where Λ_θ denotes the helicity density at an angle θ . After some algebra (see Appendix C), we obtain

$$P_l^m(\cos\theta) \frac{\partial P_l^m(\cos\theta)}{\partial \cos\theta} = 0 \implies \langle \Lambda \rangle = \Lambda_\theta, \quad (17)$$

where $P_l^m(\cos\theta)$ are the associated Legendre polynomials [45]. This is another key result of the present work. The helicity expectation value can indeed be computed from a single measurement of the helicity density at a specific angle θ . Our result implies that for a cylindrically symmetric scatterer whose response can be well-described by a single multipolar order, l , if we excite it with an illumination with a fixed total angular momentum, m , Eq. (17) specifies the angle at which the helicity density is equal to its expected value. Thus, and

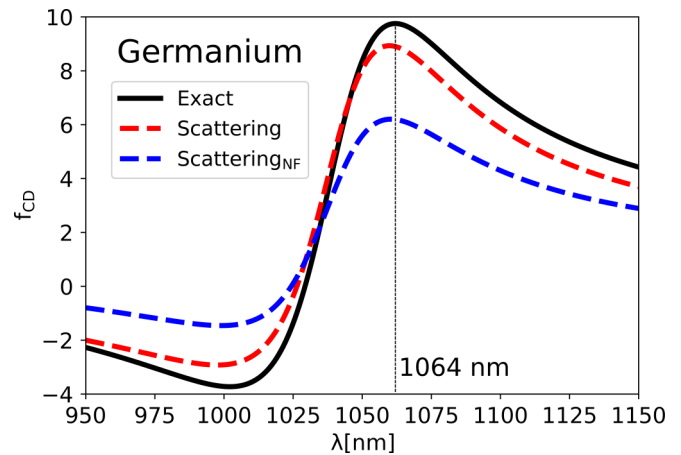


FIG. 3. f_{CD} for a Germanium dipolar sphere ($m = 4.25$) with radii $a = 118$ nm under the illumination of a circularly polarized plane-wave. The integrating sphere has a radius of 121 nm. Exact f_{CD} (solid black). Scattering f_{CD} (dashed red) with $\ell = m = 1$, so Eq. (18) is used. f_{CD} calculated only from the near field of the scattered field (dashed blue). The maximum value of f_{CD} occurs at $\lambda = 1064$ nm.

according to Eq. (16), for lossless and cylindrically symmetric targets, we can infer the f_{CD} factor by just considering two far-field measurements: extinction cross-section, in the forward direction, and helicity density, at an angle θ specified by Eq. (17) [55].

For instance, if we consider the typical case of a cylindrically symmetric dipolar target ($l = 1$) under a circularly polarized plane-wave illumination ($m = \pm 1$), Eq. (17) yields that the angle we should look at is $\theta = \pi/2$. In this case, the f_{CD} factor reads for lossless and cylindrical dipolar antennas as

$$f_{\text{CD}} \sim 1 + \frac{\pi G_{h_l h_l}}{\lambda^2} \Lambda_{\pi/2} \sigma_{\text{ext}}. \quad (18)$$

Table I summarizes the primary expressions discussed in this letter, particularized for plane-wave illumination and spherical Mie scatterers. Note that the electric and magnetic Mie coefficients emerge since we are dealing with a high refractive index spherical object [47]. Nonetheless, one can tackle other geometries using the T-matrix formalism [56,57]. It is important to emphasize that in Table I, one can find the exact multipolar expansion and the scattering approximation for f_{CD} . Moreover, one can also see the expressions to capture f_{CD} from far-field measurements for both lossy and lossless achiral spherical objects. Hence, Table I can help researchers to capture the f_{CD} factor without the need to perform multiple CD experiments with suspended chiral molecules.

Interestingly, the presence of a substrate does not modify the cylindrical symmetry of the system. Hence, Eq. (17) can be applied when the cylindrical object is placed on a substrate. Thus, our expression for calculating f_{CD} , summarized in Eq. (18), can be used when a substrate is considered.

To conclude this work, we present an illustrative example that encompasses our findings. Indeed, in Fig. 3, we compare different approximations for the f_{CD} factor of a Germanium (Ge) dipolar sphere with a radius of $a = 118$ nm. Note that $r = a + \delta_x = 121$ nm, so $\delta_x = 3$ nm. As shown in Fig. 3, the exact result (solid black) and the scattering approximation

for $\ell = m = 1$ (dashed red) agree well, with a relative error always below 10%. This indicates that our method, which involves measuring helicity at the right angle and the extinction cross-section, can accurately capture the f_{CD} factor for spherical dipolar particles [58]. However, the near-field contribution of the scattered field produces worse results, as shown by the blue dashed curve in Fig. 3. Previous studies have used the near-field approximation of the scattered fields to provide analytical expressions for the f_{CD} factor [8,27,46], but our findings suggest that this approach may not be suitable for accurate calculations. In this regard, see Appendix D for more details on the near-field approximation of the f_{CD} factor.

In conclusion, we have derived an exact multipolar expression of f_{CD} for scatterers of any form, shape, and material. This is the very first exact expression of f_{CD} that allows researchers to anticipate experimentally how efficient is an achiral antenna in enhancing molecular CD signals prior to running CD measurements involving any chiral molecules. As a matter of fact, we have derived f_{CD} under general illumination conditions. In other words, we have not restricted ourselves to a circularly polarized plane-wave excitation in our derivation. Hence, our results can find potential applications in developing novel enhanced chiral sensing techniques using structured fields.

In addition to this, our work unveils a new experimental method to determine the capability of an optical antenna to enhance the CD spectra of a set of molecules surrounding it. This experimental method only requires two measurements in the far field: the scattering cross-section and the helicity expectation value. Moreover, we proved that by measuring extinction (in the forward direction) and the density of helicity at the perpendicular direction to the incident wave, one could anticipate how efficient the achiral dipolar antenna would be at enhancing molecular CD spectra. In fact, it has been recently demonstrated that a local and single measurement of the degree of circular polarization in the far-field enables quantifying near-field CD enhancements [59]. In particular, it has been proved for a monodisperse solution of Silicon nanoresonators. We believe that the simplicity of these measurements will pave the way for experimental verification and characterization of building blocks for CD enhancement from far-field measurements and, thus, may give rise to novel developments in the field of chiral light-matter interactions.

ACKNOWLEDGMENTS

J.O.T. acknowledges support from the Juan de la Cierva fellowship No. FJC2021-047090-I of MCIN/AEI/10.13039/501100011033 and NextGenerationEU/PRTR. J.O.T. acknowledges support from Project No. PID2022-137569NB-C43 of the Spanish Ministerio de Ciencia, Innovación y Universidades (MICIU) and Dr. Cristina Sanz-Fernández for her help with the figures. J.L.A., J.O.T., and G.M.T acknowledge support from Project No. PID2022-143268NB-I00 of the Spanish Ministerio de Ciencia, Innovación y Universidades (MICIU). J.L.A., and A.G.E. acknowledge support from Project No. PID2022-142008NB-I00 of the Spanish Ministerio de Ciencia, Innovación y Universidades (MICIU). We received funding from the IKUR Strategy under the collaboration agreement between Ikerbasque Foundation and DIPC on

behalf of the Department of Education of the Basque Government, as well the Basque Government Elkartek program (No. KK-2023/00016) and the Centros Severo Ochoa AEI/CEX2018-000867-S from the Spanish Ministerio de Ciencia e Innovación.

APPENDIX A: MULTIPOLAR ELECTROMAGNETIC FIELDS IN A WELL-DEFINED HELICITY BASIS

1. Incident electromagnetic fields

First, we need to write down the electromagnetic fields to calculate the surface-enhanced circular dichroism (CD). The most generic expression of the incident electromagnetic fields are given by

$$\mathbf{E}_{\text{inc}}(\mathbf{r}) = \sum_{l=0}^{\infty} \sum_{m=-l}^{+l} g_{lm}^e N_{lm}^j(\mathbf{r}) + g_{lm}^m \mathbf{M}_{lm}^j(\mathbf{r}), \quad (\text{A1})$$

$$\mathbf{ZH}_{\text{inc}}(\mathbf{r}) = \sum_{l=0}^{\infty} \sum_{m=-l}^{+l} g_{lm}^e \mathbf{M}_{lm}^j(\mathbf{r}) - g_{lm}^m N_{lm}^j(\mathbf{r}), \quad (\text{A2})$$

where g_{lm}^e and g_{lm}^m stands for the incident electric and magnetic beam's shape coefficients, respectively, and

$$\begin{aligned} \mathbf{M}_{lm}^j(\mathbf{r}) &= j_l(kr) \mathbf{X}_{lm}(\mathbf{r}), & N_{lm}^j(\mathbf{r}) &= \frac{i \nabla \times \mathbf{M}_{lm}^j(\mathbf{r})}{k}, \\ \mathbf{X}_{lm}(\mathbf{r}) &= \frac{\mathbf{L} Y_{lm}(\theta, \varphi)}{\sqrt{l(l+1)}}. \end{aligned} \quad (\text{A3})$$

Here $\mathbf{M}_{lm}^j(\mathbf{r})$ and $N_{lm}^j(\mathbf{r})$ are (incident) Hansen's multipoles [45], $j_l(kr)$ are the spherical Bessel functions, k being the radiation wavelength, and \mathbf{r} the observation point. Moreover, $Y_{lm}(\theta, \varphi)$ are the spherical harmonics, θ and φ being the polar and azimuthal angles, and $\mathbf{L} = \{-i\mathbf{r} \times \nabla\}$ is the total angular momentum operator. At this point, let us consider an arbitrary incident electromagnetic field with well-defined helicity, $\sigma = \pm 1$. Mathematically, we can write this well-defined helicity field as

$$\begin{aligned} \mathbf{E}_{\text{inc}}^{\sigma}(\mathbf{r}) &= \frac{\mathbf{E}_{\text{inc}}(\mathbf{r}) + \sigma i \mathbf{ZH}_{\text{inc}}(\mathbf{r})}{2} \\ &= \sum_{l=0}^{\infty} \sum_{m=-l}^{+l} \left(\frac{g_{lm}^e - i\sigma g_{lm}^m}{\sqrt{2}} \right) \left(\frac{N_{lm}^j(\mathbf{r}) + i\sigma \mathbf{M}_{lm}^j(\mathbf{r})}{\sqrt{2}} \right) \\ &= \sum_{l=0}^{\infty} \sum_{m=-l}^{+l} C_{lm}^{\sigma} \Psi_{lm}^{\sigma}(\mathbf{r}), \end{aligned} \quad (\text{A4})$$

where

$$C_{lm}^{\sigma} = \frac{g_{lm}^e - i\sigma g_{lm}^m}{\sqrt{2}} \quad \text{and} \quad \Psi_{lm}^{\sigma}(\mathbf{r}) = \frac{N_{lm}^j(\mathbf{r}) + i\sigma \mathbf{M}_{lm}^j(\mathbf{r})}{\sqrt{2}}. \quad (\text{A5})$$

Note that $C_{lm}^{\sigma} = g_{lm}^e = -i\sigma g_{lm}^m$. Also, let us recall that the multipoles $\Psi_{lm}^{\sigma}(\mathbf{r})$ are eigenvectors of the square of the total angular momentum J^2 , the projection of the total angular momentum in the OZ direction, J_z , and helicity $\Lambda = (1/k)\nabla \times$ operators [60–62] with eigenvalues $l(l+1)$, m , σ , respectively.

2. Scattered and total electromagnetic fields

At this point, let us consider the scattered electromagnetic fields. The most generic expression of these fields is given by

$$\mathbf{E}_{\text{sca}}^{\sigma}(\mathbf{r}) = \sum_{l=0}^{\infty} \sum_{m=-l}^{+l} a_{lm}^{\sigma} \mathbf{N}_{lm}^h(\mathbf{r}) + b_{lm}^{\sigma} \mathbf{M}_{lm}^h(\mathbf{r}), \quad (\text{A6})$$

$$\mathbf{ZH}_{\text{sca}}^{\sigma}(\mathbf{r}) = \sum_{l=0}^{\infty} \sum_{m=-l}^{+l} a_{lm}^{\sigma} \mathbf{M}_{lm}^h(\mathbf{r}) - b_{lm}^{\sigma} \mathbf{N}_{lm}^h(\mathbf{r}), \quad (\text{A7})$$

where a_{lm}^{σ} and b_{lm}^{σ} stand for the electric and magnetic scattering coefficients, respectively. Notice that a_{lm}^{σ} and b_{lm}^{σ} depend on the incident illumination. As a result, we have explicitly indicated the σ -dependency. Moreover,

$$\mathbf{M}_{lm}^h(\mathbf{r}) = h_l(kr) \mathbf{X}_{lm}(\mathbf{r}), \quad \mathbf{N}_{lm}^h(\mathbf{r}) = \frac{\mathbf{i}\nabla \times \mathbf{M}_{lm}^h(\mathbf{r})}{k}, \quad (\text{A8})$$

where $\mathbf{M}_{lm}^h(\mathbf{r})$ and $\mathbf{N}_{lm}^h(\mathbf{r})$ are (scattered) Hansen's multipoles [45] and $h_l(kr)$ are the spherical Hankel functions. Following the steps done in Eq. (A4), the electric field reads as

$$\begin{aligned} \mathbf{E}_{\text{sca}}^{\sigma\sigma'}(\mathbf{r}) &= \frac{\mathbf{E}_{\text{sca}}^{\sigma}(\mathbf{r}) + \sigma' \mathbf{i} \mathbf{ZH}_{\text{sca}}^{\sigma}(\mathbf{r})}{2} \\ &= \sum_{l=0}^{\infty} \sum_{m=-l}^{+l} \left(\frac{a_{lm}^{\sigma} - \mathbf{i}\sigma' b_{lm}^{\sigma}}{\sqrt{2}} \right) \left(\frac{\mathbf{N}_{lm}^h(\mathbf{r}) + \mathbf{i}\sigma' \mathbf{M}_{lm}^h(\mathbf{r})}{\sqrt{2}} \right) \\ &= \sum_{l=0}^{\infty} \sum_{m=-l}^{+l} D_{lm}^{\sigma\sigma'} \Phi_{lm}^{\sigma'}(\mathbf{r}), \end{aligned} \quad (\text{A9})$$

where

$$D_{lm}^{\sigma\sigma'} = \frac{a_{lm}^{\sigma} - \mathbf{i}\sigma' b_{lm}^{\sigma}}{\sqrt{2}} \quad \text{and} \quad \Phi_{lm}^{\sigma'}(\mathbf{r}) = \frac{\mathbf{N}_{lm}^h(\mathbf{r}) + \mathbf{i}\sigma' \mathbf{M}_{lm}^h(\mathbf{r})}{\sqrt{2}}. \quad (\text{A10})$$

To conclude Appendix A, let us write the total electromagnetic fields. These are given by the additive sum of the incident

and scattered electromagnetic fields. Hence, by taking into account both Eqs. (A4) and (A9), we can straightforwardly write

$$\mathbf{E}_{\text{tot}}^{\sigma}(\mathbf{r}) = \sum_{\sigma'=\pm 1} \mathbf{E}_{\text{tot}}^{\sigma\sigma'}(\mathbf{r}), \quad \mathbf{i} \mathbf{ZH}_{\text{tot}}^{\sigma}(\mathbf{r}) = \sum_{\sigma'=\pm 1} \sigma' \mathbf{E}_{\text{tot}}^{\sigma\sigma'}(\mathbf{r}), \quad (\text{A11})$$

with

$$\mathbf{E}_{\text{tot}}^{\sigma\sigma'}(\mathbf{r}) = \mathbf{E}_{\text{sca}}^{\sigma\sigma'}(\mathbf{r}) + \mathbf{E}_{\text{inc}}^{\sigma}(\mathbf{r}) \delta_{\sigma\sigma'}, \quad (\text{A12})$$

where $\delta_{\sigma\sigma'}$ is a Kronecker δ . Next, we will use the orthogonality expressions that satisfy both the incident and scattered electromagnetic fields to compute the exact multipolar expansion of the CD enhancement factor.

APPENDIX B: AN EXACT MULTIPOLAR EXPANSION OF f_{CD} BEYOND THE PLANE-WAVE PICTURE

1. An exact multipolar expansion of f_{CD} : Orthogonality relations of well-defined helicity multipoles

To derive an exact multipolar expansion of the CD enhancement factor, f_{CD} , beyond the plane-wave picture, we need to know the orthogonality relations that satisfy both incident and scattered electromagnetic fields over an integrating sphere surrounding the object under illumination. To that end, we need first to calculate the set of orthogonality relations fulfilled by multipoles with well-defined helicity. That is, we need the orthogonality relations between incident $\{\Psi_{lm}^{\sigma}, \Psi_{l'm'}^{\sigma}\}$, interference $\{\Psi_{lm}^{\sigma}, \Phi_{l'm'}^{\sigma}\}$, and scattering $\{\Phi_{lm}^{\sigma}, \Phi_{l'm'}^{\sigma}\}$ terms, according to Eq. (7). Fortunately, all these relations can be derived from Jackson's third edition book. Let us start this section by transcribing Eq. (10.48) that can be found on page 472 of Ref. [45]:

$$\int_{\Omega} N_{lm}^{f*} \cdot N_{l'm'}^g d\Omega = \delta_{ll'} \delta_{mm'} \left(f_l^*(u) g_l(u) + \frac{1}{u^2} \frac{\partial}{\partial u} \left\{ u f_l^*(u) \frac{\partial}{\partial u} [u g_l(u)] \right\} \right), \quad \int_{\Omega} M_{lm}^{f*} \cdot M_{l'm'}^g d\Omega = f_l^*(u) g_l(u) \delta_{ll'} \delta_{mm'}. \quad (\text{B1})$$

Here $u = kr$ denotes the optical radius of the integrating sphere and $\{\delta_{ll'}, \delta_{mm'}\}$ are Kronecker δ s. Notice that $\{f_l(u), g_l(u)\}$ denote either Bessel or Hankel spherical functions, namely, $j_l(u)$ and $h_l(u)$ [45], depending on the nature of the field: incident or scattered, respectively.

At this point, we have already learned that multipoles with well-defined helicity $\{\Psi_{lm}^{\sigma}, \Phi_{lm}^{\sigma}\}$ are constructed by a linear combination of the Hansel multipoles [see the right-hand side of Eqs. (A5) and (A10)]. As a result, we can write from Eq. (B1)

$$\int_{\Omega} (\Psi_{l'm'}^{\sigma})^* \cdot \Psi_{lm}^{\sigma} d\Omega = G_{j_l j_l} \delta_{ll'} \delta_{mm'}, \quad \int_{\Omega} (\Phi_{l'm'}^{\sigma})^* \cdot \Phi_{lm}^{\sigma} d\Omega = G_{h_l h_l} \delta_{ll'} \delta_{mm'}, \quad \int_{\Omega} (\Psi_{l'm'}^{\sigma})^* \cdot \Phi_{lm}^{\sigma} d\Omega = G_{j_l h_l} \delta_{ll'} \delta_{mm'}, \quad (\text{B2})$$

with

$$G_{f_l g_l} = \frac{1}{2} \left(2 f_l^*(u) g_l(u) + \frac{1}{u^2} \frac{\partial}{\partial u} \left\{ u f_l^*(u) \frac{\partial}{\partial u} [u g_l(u)] \right\} \right). \quad (\text{B3})$$

Now, we can rewrite Eq. (B3) to get rid of second derivatives by making use of fundamental properties of the Riccati-Bessel functions [63]. In particular, we can write

$$G_{j_l j_l} = \frac{1}{2} \left(j_l^2(u) \left[1 + \frac{l(l+1)}{u^2} \right] + \frac{1}{u^2} \left\{ \frac{\partial}{\partial u} [u j_l(u)] \right\}^2 \right) \quad G_{h_l h_l} = \frac{1}{2} \left\{ |h_l(u)|^2 \left[1 + \frac{l(l+1)}{u^2} \right] + \frac{1}{u^2} \left| \frac{\partial}{\partial u} [u h_l(u)] \right|^2 \right\}, \quad (\text{B4})$$

$$G_{jh_l} = \frac{1}{2} \left(j_l(u) h_l(u) \left[1 + \frac{l(l+1)}{u^2} \right] + \frac{1}{u^2} \left\{ \frac{\partial}{\partial u} [u j_l(u)] \frac{\partial}{\partial u} [u h_l(u)] \right\} \right), \quad (\text{B5})$$

where $\frac{\partial}{\partial u} [u f_l(u)] = u f_{l-1}(u) - l f_l(u)$ is satisfied for $f(u) = \{j_l(u), h_l(u)\}$.

2. An exact multipolar expansion of f_{CD} : From the helicity basis to the standard electric and magnetic multipolar expansion

At this stage, we have all ingredients to calculate the exact multipolar expansion of f_{CD} . The starting point of this section will be Eq. (7). According to Eq. (7), we need the orthogonality relations that satisfy the Riemann-Silberstein representation of the incident and scattered electromagnetic fields:

$$\tilde{C}_{\text{inc}}^\sigma = \int_{\Omega} C_{\text{inc}}^\sigma(\mathbf{r}) d\Omega = \int_{\Omega} \sigma |\mathbf{E}_{\text{inc}}^\sigma(\mathbf{r})|^2 d\Omega, \quad (\text{B6})$$

$$\tilde{C}_{\text{sca}}^\sigma = \int_{\Omega} C_{\text{sca}}^\sigma(\mathbf{r}) d\Omega = \int_{\Omega} (|\mathbf{E}_{\text{sca}}^{\sigma+}(\mathbf{r})|^2 - |\mathbf{E}_{\text{sca}}^{\sigma-}(\mathbf{r})|^2) d\Omega, \quad (\text{B7})$$

$$C_{\text{int}}^\sigma = \int_{\Omega} \tilde{C}_{\text{int}}^\sigma(\mathbf{r}) d\Omega = 2\sigma \int_{\Omega} \text{Re}\{\mathbf{E}_{\text{inc}}^{\sigma*}(\mathbf{r}) \cdot \mathbf{E}_{\text{sca}}^{\sigma\sigma}(\mathbf{r})\} d\Omega. \quad (\text{B8})$$

These orthogonality relations can be computed by combining Eqs. (A4) and (A9) with Eq. (B2). In fact, and after some algebraic manipulations, it can be shown that

$$\begin{aligned} \tilde{C}_{\text{inc}}^\sigma &= \sigma \sum_{lm} |C_{lm}^\sigma|^2 G_{jh_l}, \\ \tilde{C}_{\text{sca}}^\sigma &= \sum_{lm} (|D_{lm}^{\sigma+}|^2 - |D_{lm}^{\sigma-}|^2) G_{jh_l}, \\ \tilde{C}_{\text{int}}^\sigma &= 2\sigma \sum_{lm} \text{Re}\{C_{lm}^{\sigma*} D_{lm}^{\sigma\sigma} G_{jh_l}\}. \end{aligned} \quad (\text{B9})$$

Now, let us obtain a closed relation of the optical chirality enhancements in terms of the electric and magnetic scattering coefficients. After some algebra, we arrive to

$$f_{\text{CD}} = 1 + \frac{\tilde{C}_{\text{sca}}^\sigma + \tilde{C}_{\text{int}}^\sigma}{\tilde{C}_{\text{inc}}^\sigma}, \quad (\text{B10})$$

with

$$\begin{aligned} \tilde{C}_{\text{inc}}^\sigma &= \sigma \sum_{lm} |C_{lm}^\sigma|^2 G_{jh_l}, \quad \tilde{C}_{\text{sca}}^\sigma = -2 \sum_{lm} \text{Im}\{a_{lm}^\sigma b_{lm}^{\sigma*}\} G_{jh_l}, \\ \tilde{C}_{\text{int}}^\sigma &= \sqrt{2} \sum_{lm} \text{Re}\{C_{lm}^{\sigma*} (a_{lm}^\sigma - i\sigma b_{lm}^\sigma) G_{jh_l}\}. \end{aligned} \quad (\text{B11})$$

APPENDIX C: EXTRACTING THE HELICITY EXPECTATION VALUE FROM A SINGLE MEASUREMENT OF ITS LOCAL DENSITY

In this Appendix, we derive the condition given in Eq. (17), that relates the local density of helicity at a certain angle, $\Lambda_{\theta, \phi}$, with the helicity expectation value, $\langle \Lambda \rangle$. For that aim, we should first define the local density of helicity, which we consider to be given in the far field by

$$\Lambda_{\theta, \phi} \equiv \lim_{kr \rightarrow \infty} \frac{|\mathbf{E}_{\text{sca}}^{\sigma+}(r, \theta, \varphi)|^2 - |\mathbf{E}_{\text{sca}}^{\sigma-}(r, \theta, \varphi)|^2}{|\mathbf{E}_{\text{sca}}^{\sigma+}(r, \theta, \varphi)|^2 + |\mathbf{E}_{\text{sca}}^{\sigma-}(r, \theta, \varphi)|^2}, \quad (\text{C1})$$

where $\mathbf{E}_{\text{sca}}^{\sigma\sigma'}(r, \theta, \varphi)$ is the scattered field written in terms of electromagnetic modes with well-defined helicity. From Eq. (C1), we notice that we require the asymptotic behavior of $\mathbf{E}_{\text{sca}}^{\sigma\sigma'}(r, \theta, \varphi)$ in the far-field limit. For that aim, we need first to calculate how Hansel multipoles behave in the far-field limit. After some algebra, we arrive to

$$\begin{aligned} \lim_{kr \rightarrow \infty} \mathbf{N}_{lm}^h(\mathbf{r}) &= -i \frac{e^{ikr}}{kr} \frac{(-i)^{l+1}}{\sqrt{l(l+1)}} \boldsymbol{\xi}_{lm}(\theta, \varphi), \\ \lim_{kr \rightarrow \infty} \mathbf{M}_{lm}^h(\mathbf{r}) &= -i \frac{e^{ikr}}{kr} \frac{(-i)^{l+1}}{\sqrt{l(l+1)}} \boldsymbol{\eta}_{lm}(\theta, \varphi), \end{aligned} \quad (\text{C2})$$

where $\boldsymbol{\xi}_{lm}(\theta, \varphi) = r \nabla Y_{lm}(\theta, \varphi)$ and $\boldsymbol{\eta}_{lm}(\theta, \varphi) = \hat{r} \times \boldsymbol{\xi}_{lm}(\theta, \varphi)$. Now, the far-field expression of the electromagnetic field scattered by an arbitrary sample can be computed [64]:

$$\mathbf{E}_{\text{sca}}^{\sigma\sigma'}(r, \theta, \varphi) = -i \frac{e^{ikr}}{kr} \frac{(-i)^{\ell+1}}{\sqrt{\ell(\ell+1)}} D_{\ell m}^{\sigma\sigma'} \left(\frac{\boldsymbol{\xi}_{\ell m}(\theta, \varphi) + i\sigma' \boldsymbol{\eta}_{\ell m}(\theta, \varphi)}{\sqrt{2}} \right). \quad (\text{C3})$$

Substituting the scattered field in Eq. (C3) into the expression of the helicity density given by Eq. (C1), we obtain for fixed l and m values:

$$\Lambda_\theta = 2 \frac{\text{Im}(a_{lm}^{\sigma*} b_{lm}^\sigma) [|\boldsymbol{\xi}_{lm}|^2 + |\boldsymbol{\eta}_{lm}|^2] - [|a_{lm}^\sigma|^2 + |b_{lm}^\sigma|^2] \text{Im}(\boldsymbol{\xi}_{lm}^* \cdot \boldsymbol{\eta}_{lm})}{[|a_{lm}^\sigma|^2 + |b_{lm}^\sigma|^2] [|\boldsymbol{\xi}_{lm}|^2 + |\boldsymbol{\eta}_{lm}|^2] - 4 \text{Im}(a_{lm}^{\sigma*} b_{lm}^\sigma) \text{Im}(\boldsymbol{\xi}_{lm}^* \cdot \boldsymbol{\eta}_{lm})}. \quad (\text{C4})$$

The type of scatterers which may be described by fixed l and m values are cylindrically symmetric particles, illuminated by a beam with a well-defined angular momentum, m , and with a non multipolar response. Due to the cylindrical symmetry of the scatterers, helicity density cannot depend on φ variable. This is the reason why we have chosen to write helicity density as Λ_θ in Eq. (C4). Crucially, whenever $\text{Im}(\boldsymbol{\xi}_{lm}^* \cdot \boldsymbol{\eta}_{lm}) = 0$, one recovers the expression of the helicity expectation value, i.e.,

$$\text{Im}(\boldsymbol{\xi}_{lm}^* \cdot \boldsymbol{\eta}_{lm}) = 0 \implies \Lambda_\theta = \langle \Lambda \rangle = 2 \frac{\text{Im}(a_{lm}^{\sigma*} b_{lm}^\sigma)}{|a_{lm}^\sigma|^2 + |b_{lm}^\sigma|^2}. \quad (\text{C5})$$

Importantly, the condition $\text{Im}(\xi_{lm}^* \cdot \eta_{lm}) = 0$ is purely geometrical, i.e., does not depend on the particular response of the scatterer. This fact makes the expression completely general and applicable to any type of cylindrical sample whose response is well-described by a fixed l . Thus, for this type of scatterers, there are locations in the far field at which the helicity density is equal to the helicity expectation value. The specific sites at which $\langle \Lambda \rangle = \Lambda_\theta$ are obtained by finding the solutions to the equation $\text{Im}(\xi_{lm}^* \cdot \eta_{lm}) = 0$. More explicitly, we have that the vector and scalar spherical harmonics are written as

$$\xi_{lm}(\theta, \varphi) = \frac{\partial Y_{lm}(\theta, \varphi)}{\partial \theta} \hat{u}_\theta + \frac{1}{\sin \theta} \frac{\partial Y_{lm}(\theta, \varphi)}{\partial \varphi} \hat{u}_\varphi, \quad (\text{C6})$$

$$\eta_{lm}(\theta, \varphi) = \frac{\partial Y_{lm}(\theta, \varphi)}{\partial \theta} \hat{u}_\varphi - \frac{1}{\sin \theta} \frac{\partial Y_{lm}(\theta, \varphi)}{\partial \varphi} \hat{u}_\theta, \quad (\text{C7})$$

$$Y_{lm}(\theta, \varphi) = \sqrt{\frac{2l+1}{4\pi} \frac{(l-m)!}{(l+m)!}} P_l^m(\cos \theta) e^{im\varphi}, \quad (\text{C8})$$

where $P_l^m(\cos \theta)$ are the associated Legendre polynomials. With the definitions above it is straightforward to check that

$$P_l^m(\cos \theta) \frac{\partial P_l^m(\cos \theta)}{\partial \cos \theta} = 0 \implies \text{Im}(\xi_{lm}^* \cdot \eta_{lm}) = 0. \quad (\text{C9})$$

In conclusion, for fixed values of l and m , there is an angle θ , given by the transcendental equation above, at which the helicity density, Λ_θ , is equal to the helicity expectation value, $\langle \Lambda \rangle$.

APPENDIX D: NEAR-FIELD APPROXIMATION OF $G_{h_1 h_1}$

Let us consider the following limit,

$$\begin{aligned} \lim_{u \ll 1} G_{h_1 h_1} &= \lim_{u \ll 1} \frac{1}{2} \left[2|h_l(u)|^2 + \frac{1}{u^2} \frac{\partial}{\partial u} \left(u h_l^*(u) \frac{\partial}{\partial u} (u h_l(u)) \right) \right] \\ &= \lim_{u \ll 1} \frac{[|h_l(u)|^2 + l(l+1)|h_l(u)|^2]}{2u^2}, \end{aligned} \quad (\text{D1})$$

where $u = kr$. Now, let us consider $l = 1$ in the previous expression. That is

$$\begin{aligned} \lim_{kr \ll 1} G_{h_1 h_1} &= \lim_{kr \ll 1} \frac{3}{2} \left(\frac{|h_1(kr)|^2}{(kr)^2} \right) = \frac{3}{2} \left(\frac{1}{(kr)^6} \right), \quad \text{since} \\ h_1(u) &= \frac{e^{-iu}}{u} \left(1 + \frac{1}{u} \right). \end{aligned} \quad (\text{D2})$$

At this point, let us insert the near-field limit of $G_{h_1 h_1}$ into the f_{CD} factor of a dipolar sphere under plane-wave illumination. This operation yields

$$f_{\text{CD}} = 1 + \frac{9\text{Re}\{a_1 b_1^*\}}{2(kr)^6}. \quad (\text{D3})$$

Equation (D3) is exactly Eq. (9) of Ref. [8]. Note that we have performed many approximations to get Equation (D3) from the exact expression of f_{CD} . These are: (1) electric and magnetic dipolar regime, (2) plane-wave illumination, (3) homogeneous sphere, and (4) near-field limit. Note that Equation (D3) corresponds to the dashed blue curve (Scattering_{NF}) in Fig. 3.

-
- [1] J. Watson, *The Double Helix* (Hachette, UK, 2012)
- [2] M. G. Calkin, An invariance property of the free electromagnetic field, *Am. J. Phys.* **33**, 958 (1965).
- [3] N. Yu and F. Capasso, Flat optics with designer metasurfaces, *Nat. Mater.* **13**, 139 (2014).
- [4] D. Wen, S. Chen, F. Yue, K. Chan, M. Chen, M. Ardron, K. F. Li, P. W. H. Wong, K. W. Cheah, E. Y. B. Pun *et al.*, Metasurface device with helicity-dependent functionality, *Adv. Opt. Mater.* **4**, 321 (2016).
- [5] J. M. Abendroth, M. L. Solomon, D. R. Barton III, M. S. El Hadri, E. E. Fullerton, and J. A. Dionne, Helicity-preserving metasurfaces for magneto-optical enhancement in ferromagnetic [Pt/Co]N films, *Adv. Opt. Mater.* **8**, 2001420 (2020).
- [6] C. Zhang, G. Wang, H.-X. Xu, X. Zhang, and H.-P. Li, Helicity-dependent multifunctional metasurfaces for full-space wave control, *Adv. Opt. Mater.* **8**, 1901719 (2020).
- [7] X. Zambrana-Puyalto and N. Bonod, Tailoring the chirality of light emission with spherical Si-based antennas, *Nanoscale* **8**, 10441 (2016).
- [8] A. García-Etxarri and J. A. Dionne, Surface-enhanced circular dichroism spectroscopy mediated by nonchiral nanoantennas, *Phys. Rev. B* **87**, 235409 (2013).
- [9] A. García-Etxarri, J. M. Ugalde, J. J. Sáenz, and V. Mujica, Field-mediated chirality information transfer in molecule-nanoparticle hybrids, *J. Phys. Chem. C* **124**, 1560 (2020).
- [10] Z. Fan and A. O. Govorov, Plasmonic circular dichroism of chiral metal nanoparticle assemblies, *Nano Lett.* **10**, 2580 (2010).
- [11] J. García-Guirado, M. Svedendahl, J. Puigdollers, and R. Quidant, Enantiomer-selective molecular sensing using racemic nanoplasmonic arrays, *Nano Lett.* **18**, 6279 (2018).
- [12] L. V. Poulikakos, P. Gutsche, K. M. McPeak, S. Burger, J. Niegemann, C. Hafner, and D. J. Norris, Optical chirality flux as a useful far-field probe of chiral near fields, *ACS Photon.* **3**, 1619 (2016).
- [13] L. V. Poulikakos, P. Thureja, A. Stollmann, E. De Leo, and D. J. Norris, Chiral light design and detection inspired by optical antenna theory, *Nano Lett.* **18**, 4633 (2018).
- [14] A. García-Etxarri, R. Gómez-Medina, L. S. Froufe-Pérez, C. López, L. Chantada, F. Scheffold, J. Aizpurua, M. Nieto-Vesperinas, and J. J. Sáenz, Strong magnetic response of submicron silicon particles in the infrared, *Opt. Express* **19**, 4815 (2011).
- [15] J. Olmos-Trigo, D. R. Abujetas, C. Sanz-Fernández, J. A. Sánchez-Gil, and J. J. Sáenz, Optimal backward light scattering by dipolar particles, *Phys. Rev. Res.* **2**, 013225 (2020).
- [16] M. L. Tseng, Y. Jahani, A. Leitis, and H. Altug, Dielectric metasurfaces enabling advanced optical biosensors, *ACS Photon.* **8**, 47 (2021).
- [17] L. A. Warning, A. R. Miandashti, L. A. McCarthy, Q. Zhang, C. F. Landes, and S. Link, Nanophotonic approaches for chirality sensing, *ACS Nano* **15**, 15538 (2021).
- [18] Y. Chen, C. Zhao, Y. Zhang, and C.-W. Qiu, Integrated molar chiral sensing based on high-Q metasurface, *Nano Lett.* **20**, 8696 (2020).

- [19] J. Ni, S. Liu, D. Wu, Z. Lao, Z. Wang, K. Huang, S. Ji, J. Li, Z. Huang, Q. Xiong *et al.*, Gigantic vortical differential scattering as a monochromatic probe for multiscale chiral structures, *Proc. Natl. Acad. Sci. USA* **118**, e2020055118 (2021).
- [20] Y. Chen, W. Chen, X. Kong, D. Wu, J. Chu, and C.-W. Qiu, Can weak chirality induce strong coupling between resonant states? *Phys. Rev. Lett.* **128**, 146102 (2022).
- [21] E. S. A. Goerlitzer, M. Zapata-Herrera, E. Ponomareva, D. Feller, A. Garcia-Etxarri, M. Karg, J. Aizpurua, and N. Vogel, Molecular-induced chirality transfer to plasmonic lattice modes, *ACS Photon.* **10**, 1821 (2023).
- [22] J. Hu, M. Lawrence, and J. A. Dionne, High quality factor dielectric metasurfaces for ultraviolet circular dichroism spectroscopy, *ACS Photon.* **7**, 36 (2020).
- [23] E. Hendry, T. Carpy, J. Johnston, M. Popland, R. V. Mikhaylovskiy, A. J. Laphorn, S. M. Kelly, L. D. Barron, N. Gadegaard, and M. J. N. N. Kadodwala, Ultrasensitive detection and characterization of biomolecules using superchiral fields, *Nat. Nanotechnol.* **5**, 783 (2010).
- [24] C. Kelly, L. Khosravi Khorashad, N. Gadegaard, L. D. Barron, A. O. Govorov, A. S. Karimullah, and M. Kadodwala, Controlling metamaterial transparency with superchiral fields, *ACS Photon.* **5**, 535 (2018).
- [25] W. Zhang, T. Wu, R. Wang, and X. Zhang, Amplification of the molecular chiroptical effect by low-loss dielectric nanoantennas, *Nanoscale* **9**, 5701 (2017).
- [26] K. Yao and Y. Liu, Enhancing circular dichroism by chiral hotspots in silicon nanocube dimers, *Nanoscale* **10**, 8779 (2018).
- [27] M. Hanifeh and F. Capolino, Helicity maximization in a planar array of achiral high-density dielectric nanoparticles, *J. Appl. Phys.* **127**, 093104 (2020).
- [28] W. A. Paiva-Marques, F. Reyes Gómez, O. N. Oliveira Jr, and J. R. Mejía-Salazar, Chiral plasmonics and their potential for point-of-care biosensing applications, *Sensors* **20**, 944 (2020).
- [29] E. Mohammadi, A. Tittl, K. L. Tsakmakidis, T. V. Raziman, and A. G. Curto, Dual nanoresonators for ultrasensitive chiral detection, *ACS Photon.* **8**, 1754 (2021).
- [30] E. Hendry, R. V. Mikhaylovskiy, L. D. Barron, M. Kadodwala, and T. J. Davis, Chiral electromagnetic fields generated by arrays of nanoslits, *Nano Lett.* **12**, 3640 (2012).
- [31] M. L. Solomon, J. Hu, M. Lawrence, A. García-Etxarri, and J. A. Dionne, Enantiospecific optical enhancement of chiral sensing and separation with dielectric metasurfaces, *ACS Photon.* **6**, 43 (2019).
- [32] F. Graf, J. Feis, X. Garcia-Santiago, M. Wegener, C. Rockstuhl, and I. Fernandez-Corbaton, Achiral, helicity preserving, and resonant structures for enhanced sensing of chiral molecules, *ACS Photon.* **6**, 482 (2019).
- [33] J. Garcia-Guirado, M. Svedendahl, J. Puigdollers, and R. Quidant, Enhanced chiral sensing with dielectric nanoresonators, *Nano Lett.* **20**, 585 (2019).
- [34] J. Laso-Alonso, D. R. Abujetas, Á. Nodar, J. A. Dionne, J. J. Sáenz, G. Molina-Terriza, J. Aizpurua, and A. García-Etxarri, Surface-enhanced circular dichroism spectroscopy on periodic dual nanostructures, *ACS Photon.* **7**, 2978 (2020).
- [35] S. Droulias and L. Bougas, Absolute chiral sensing in dielectric metasurfaces using signal reversals, *Nano Lett.* **20**, 5960 (2020).
- [36] G. Rui, S. Zou, B. Gu, and Y. Cui, Surface-enhanced circular dichroism by localized superchiral hotspots in a dielectric dimer array metasurface, *J. Phys. Chem. C* **126**, 2199 (2022).
- [37] J. Feis, D. Beutel, J. Köpfler, X. Garcia-Santiago, C. Rockstuhl, M. Wegener, and I. Fernandez-Corbaton, Helicity-preserving optical cavity modes for enhanced sensing of chiral molecules, *Phys. Rev. Lett.* **124**, 033201 (2020).
- [38] M. Khanbekyan and S. Scheel, Enantiomer-discriminating sensing using optical cavities at exceptional points, *Phys. Rev. A* **105**, 053711 (2022).
- [39] J. Olmos-Trigo and X. Zambrana-Puyalto, Helicity conservation for mie optical cavities, *Phys. Rev. Appl.* **18**, 044007 (2022).
- [40] Y. Tang and A. E. Cohen, Optical chirality and its interaction with matter, *Phys. Rev. Lett.* **104**, 163901 (2010).
- [41] Notice that under the widely used illumination of circularly polarized plane-waves, we get $|C_{inc}^c(\mathbf{r})| = k\epsilon|E_0|^2/2$, E_0 denoting the amplitude of the electric field [40]. That is, we obtain a scalar that does not depend on the spatial coordinates.
- [42] J. Olmos-Trigo, M. Meléndez, R. Delgado-Buscalioni, and J. J. Sáenz, Sectoral multipole focused beams, *Opt. Express* **27**, 16384 (2019).
- [43] I. Fernandez-Corbaton, M. Fruhnert, and C. Rockstuhl, Objects of maximum electromagnetic chirality, *Phys. Rev. X* **6**, 031013 (2016).
- [44] For the sake of simplicity and hereinafter, we assume the factor $(k\epsilon)/2$ in the definition of the density of optical chirality.
- [45] J. D. Jackson, *Classical Electrodynamics* (John Wiley & Sons, New York, NY, 1999).
- [46] S. Lee, S. J. Yoo, and Q.-H. Park, Microscopic origin of surface-enhanced circular dichroism, *ACS Photon.* **4**, 2047 (2017).
- [47] C. F. Bohren and D. R. Huffman, *Absorption and Scattering of Light by Small Particles* (John Wiley & Sons, New York, NY, 2008).
- [48] J. H. Crichton and P. L. Marston, The measurable distinction between the spin and orbital angular momenta of electromagnetic radiation, *Electr. J. Differ. Equat.* **4**, 37 (2000).
- [49] J. Olmos-Trigo, C. Sanz-Fernández, F. S. Bergeret, and J. J. Sáenz, Asymmetry and spin-orbit coupling of light scattered from subwavelength particles, *Opt. Lett.* **44**, 1762 (2019).
- [50] J. Olmos-Trigo, C. Sanz-Fernández, D. R. Abujetas, J. Laso-Alonso, N. de Sousa, A. García-Etxarri, J. A. Sánchez-Gil, G. Molina-Terriza, and J. J. Sáenz, Kerker conditions upon lossless, absorption, and optical gain regimes, *Phys. Rev. Lett.* **125**, 073205 (2020).
- [51] J. Olmos-Trigo, D. R. Abujetas, C. Sanz-Fernández, X. Zambrana-Puyalto, N. de Sousa, J. A. Sánchez-Gil, and J. J. Sáenz, Unveiling dipolar spectral regimes of large dielectric mie spheres from helicity conservation, *Phys. Rev. Res.* **2**, 043021 (2020).
- [52] J. Laso-Alonso, J. Olmos-Trigo, A. García-Etxarri, and G. Molina-Terriza, Correlations between helicity and optical losses within general electromagnetic scattering theory, *Mater. Adv.* **3**, 4179 (2022).
- [53] R. Alaee, C. Rockstuhl, and I. Fernandez-Corbaton, Exact multipolar decompositions with applications in nanophotonics, *Adv. Opt. Mater.* **7**, 1800783 (2018).
- [54] C. Sanz-Fernández, M. Molezuelas-Ferreras, J. Laso-Alonso, N. de Sousa, X. Zambrana-Puyalto, and J. Olmos-Trigo,

- Multiple Kerker anapoles in dielectric microspheres, *Laser Photon. Rev.* **15**, 2100035 (2021).
- [55] In terms of the usual Stokes parameters, the scattering cross-section is proportional to the s_0 parameter and helicity density is the ratio s_3/s_0 [52].
- [56] A. Doicu, T. Wriedt, and Y. A. Eremin, *Light Scattering by Systems of Particles: Null-field Method with Discrete Sources: Theory and Programs*, Vol. 124 (Springer, Berlin, 2006).
- [57] K. M. Czajkowski and T. J. Antosiewicz, Local versus bulk circular dichroism enhancement by achiral all-dielectric nanoresonators, *Nanophotonics* **11**, 4287 (2022).
- [58] Note that in this spectral regime, Ge is without losses.
- [59] J. Olmos-Trigo, H. Sugimoto, and M. Fujii, Far-field detection of near-field circular dichroism enhancements induced by a nanoantenna, *Laser Photon. Rev.*, 2300948 (2024).
- [60] N. Tischler, X. Zambrana-Puyalto, and G. Molina-Terriza, The role of angular momentum in the construction of electromagnetic multipolar fields, *Eur. J. Phys.* **33**, 1099 (2012).
- [61] I. Fernandez-Corbaton, X. Zambrana-Puyalto, N. Tischler, X. Vidal, M. L. Juan, and G. Molina-Terriza, Electromagnetic duality symmetry and helicity conservation for the macroscopic Maxwell's equations, *Phys. Rev. Lett.* **111**, 060401 (2013).
- [62] J. Olmos-Trigo, M. Nieto-Vesperinas, and G. Molina-Terriza, Spheres of maximum electromagnetic chirality, [arXiv:2303.08719](https://arxiv.org/abs/2303.08719).
- [63] G. N. Watson, *A Treatise on the Theory of Bessel Functions* (Cambridge University Press, Cambridge, UK, 1995).
- [64] B. Carrascal, G. A. Estevez, P. Lee, and V. Lorenzo, Vector spherical harmonics and their application to classical electrodynamics, *Eur. J. Phys.* **12**, 184 (1991).